


Article

Neutron and Gamma Pulse Shape Discrimination by Robust Determination of the Decay Shape

Sergio Baselga ^{1,*}  and Eva Montbarbon ² 

¹ Department of Cartographic Engineering, Geodesy and Photogrammetry, Universitat Politècnica de València, Camino de Vera s/n, 46022 Valencia, Spain

² Independent Researcher, Rue Saint Maurice, 01630 Challex, France; eva.montbarbon@gmail.com

* Correspondence: serbamo@cgf.upv.es

Abstract: Neutron/gamma pulse shape discrimination (PSD) is essential in applications such as radiation source analysis, nuclear material detection, detection of pollutants in the soil and cultural heritage. Neutrons are accompanied by gamma-ray photons due to the interaction with the environment so neutron detectors require some techniques to differentiate them. There are several methods enabling such differentiation. In the current submission, a robust estimation of the decay shape is proposed as a new alternative. To do so, a robust estimator computed by a global optimization method is used. After presenting the theoretical background and explaining the required computations to be realized, the proposed method is tested in a publicly available large dataset. Evaluations of the figure of merit and the positive discrimination rate values are used to assess the degree of improvement attained. A computing code for the method, which is easily adaptable by users to their own datasets, is also provided.

Keywords: neutron and gamma discrimination; pulse shape discrimination; robust estimation; global optimization



Citation: Baselga, S.; Montbarbon, E. Neutron and Gamma Pulse Shape Discrimination by Robust Determination of the Decay Shape. *Appl. Sci.* **2024**, *14*, 5532. <https://doi.org/10.3390/app14135532>

Academic Editor: Richard Kouzes

Received: 9 June 2024

Revised: 21 June 2024

Accepted: 23 June 2024

Published: 26 June 2024



Copyright: © 2024 by the authors. Licensee MDPI, Basel, Switzerland. This article is an open access article distributed under the terms and conditions of the Creative Commons Attribution (CC BY) license (<https://creativecommons.org/licenses/by/4.0/>).

1. Introduction

Pulse shape discrimination (PSD) techniques have been widely used over the past decades to separate different radiation sources, such as fast neutrons from a gamma ray background [1]. Since a radioactive neutron source always emits gamma-ray photons, neutron detectors, such as scintillators, require techniques to differentiate both signals. The PSD techniques are based on the differences in the shapes of the scintillation signals: a gamma-ray excitation of the scintillator will give rise to a short (or prompt) decay fluorescence component, whereas a neutron interaction with the scintillator will contain both short (prompt) and long (delayed) fluorescence components [2].

The purpose of enhancing the neutron/gamma discrimination power of an organic scintillator (either liquid or plastic) can be achieved by specifically selecting the chemical composition of the material, for instance, by using a ternary fluorophore that shifts the wavelength [3]. In the field of homeland security, scintillators and discrimination techniques are of primary use in the detection of special nuclear materials (SNM) [4,5]. Some environmental challenges, such as the detection of pollutants in the soil, are also solved by making use of them [6,7]. Scintillators and PSD techniques are also employed in other fields such as non-destructive techniques for restoration studies of art works in cultural heritage [8].

One of the most common methods in PSD is the charge comparison method (CCM), see, e.g., [2,9,10]. It has the advantages of stability, reliability and simplicity in computation along with a high discrimination power [11]. It is considered as a reference to compare with more recent algorithms of neutron/gamma discrimination that have been recently proposed, such as the use of convolutional neural networks [12].

Another simple method for PSD makes use of the determination of the slope for the falling edge region [13]. It is easy to compute the slope of the straight line connecting two points (one upper threshold and one lower threshold) but it is less evident how to properly select these threshold points for them to be representative of the neutron or gamma process taking place in order to maximize the discrimination capabilities.

Since the decay observed is not linear but exponential, the approach proposed in the present paper is the determination of the exponential decay shape after the maximum amplitude for each scintillation pulse and its corresponding characterization so that it can be used for neutron and gamma discrimination. Some reasons prevent a simple computational process, however. First, the functional relationship between pulse amplitude and time is not exactly exponential, due to interactions with the observing environment. Second, it is quite common that some outlying values appear in the pulse registration. Lastly, even if the functional model was exactly exponential, the need to linearize the function before a standard adjustment might have a significantly adverse impact on the results of the estimation process.

For all these reasons, namely, the inexact functional relationship, the noise in the observational process and lack of linearity, the standard least-squares (LS) estimator may be quite adversely influenced and produce a clearly unacceptable solution. In fact, it will be shown in the application that it provides suboptimal results.

By contrast, robust estimation (RE) techniques were devised in the last decades to attain a solution for the adjustment problem that is minimally affected by the appearance of outliers in the data or systematic effects either in the data or in the model (inexactness of the functional model) while producing a solution close to the LS solution in the case of the correct functional model and the inexistence of outliers and systematic errors in the data. For a general reference on RE, the reader may consult [14]. Many robust estimators have been proposed, some showing better performance than others in coping with undesired errors of different sizes and distributions. Among them, the minimum L_1 -norm has been extensively used [15–17]. Regarding the question of how to compute the solution once the robust estimator has been selected, the so-called iteratively reweighted least squares (IRLS) scheme is the normal procedure followed due to the simplicity of recasting the RE technique in an iterative procedure based on the familiar LS scheme. As proved in [18], and recognized for many authors after, e.g., [19], this decision is at the cost of critically undermining the robust estimator capabilities for the most complicated cases (like the non-linear functional model that is needed to deal with neutron/gamma discrimination) and the use of a global optimization method is the best alternative to compute the robust estimator.

In the present work, it is shown that the determination of the shape of the neutron/gamma pulse in the decaying part can be reliably carried out by a robust estimation method (here, the minimum L_1 -norm) computed by a global optimization method (here, the simulated annealing method) and demonstrate that the estimator thus defined is able to successfully discriminate neutrons from gamma rays.

In the following section, the methods and materials in use are described, including the openly accessible dataset used for the study. Then, the results and their discussion are given, and some conclusions are drawn. In the Supplementary Materials, a computer code for the method is included, which is easily adaptable by users to their datasets.

2. Materials and Methods

2.1. Dataset

A dataset of recorded scintillation signals made accessible by [11] was used for this study. More specifically, the data to be tested was the raw signal (without any pre- or post-treatment). It consists of 14,404 scintillation pulses coming from the interaction of the well-known EJ-299-33 plastic scintillator with neutrons and gamma-rays emitted by an $^{241}\text{AmBe}$ isotope source with an average energy of 4.5 MeV. The resulting radiation field was measured using an EJ299-33 plastic scintillator and a TPS2000B digital oscilloscope. The oscilloscope worked under a sampling rate of 1 GS/s, an 8-bit vertical resolution, and

a bandwidth of 200 MHz. The trigger threshold was set at 500 mV, which corresponded approximately to an energy of 1.6 MeVee. More details about the registration process of the scintillation pulses can be found in [11] as well as in its associated Zenodo webpage (see the Data Availability Statement at the end of this paper).

2.2. Discrimination Methods

As previously mentioned, the charge comparison method is currently the most common one in PSD. In this method, the discrimination between neutrons and gamma rays is based on the analysis of the ratio R between the integrated charges of the slow Q_s and the total Q components of the scintillation pulses (Figure 1), respectively.

$$R = \frac{Q_s}{Q} \quad (1)$$

Another simple PSD method, as acknowledged in the introduction, is based on the computation of the slopes in the falling edge region, Figure 2. The slopes of the straight lines connecting two points—one upper threshold and one lower threshold for each line—are easy to compute, but it is less evident how to properly select these threshold points for them to maximize the discrimination capabilities of the neutron or gamma process taking place.

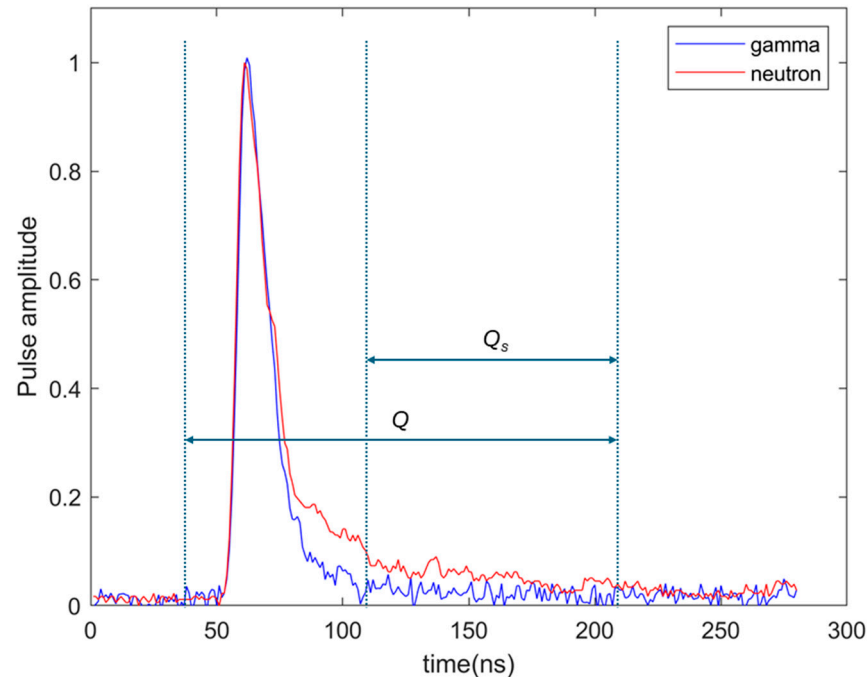


Figure 1. Values of the total integrated charge Q and the slow integrated Q_s for the charge comparison method. The ratio Q_s/Q is the main criteria of the method to classify pulses as neutron or gamma interactions with the scintillator. The ranges of integration (here, from 40 to 220 ns) have been chosen to maximize discrimination capabilities. In the figure, as in the rest of the article, pulse amplitudes are unitless after having been normalized to the range [0, 1].

Since the decay observed is not linear but exponential, the approach proposed in the present paper is the robust determination of the exponential decay shape after the maximum amplitude for each pulse, thus encapsulating the ideas in the two former methods. That is, it is assumed that the relationship between amplitude A and time t after the maximum amplitude of the pulse (decaying part) can be modeled as

$$A(t) = A_{max}e^{-\Delta t/\tau} + \delta A \quad (2)$$

where A_{max} is the maximum amplitude of the pulse, which is achieved at time t_0 (the starting time for the analysis), Δt is the difference between time t and the initial time for the analysis t_0 (that is, the time increment $t - t_0$), τ is the characteristic decay time, and δA in the residual amplitude. The latter term, amplitude δA , seems pertinent to introduce, first, because experimentally the decay does not seem to decay to zero, and, second, because neutron pulses have typically thicker tails that can be explained by the physical superposition to the main effect (prompt fluorescence) of a delayed emission which “originates from the collisional interaction of pairs of molecules (or excitons) in the lowest excited π -triplet states” [10]. The inclusion of this term effectively increases the power of discrimination, as will be shown in the numerical examples.

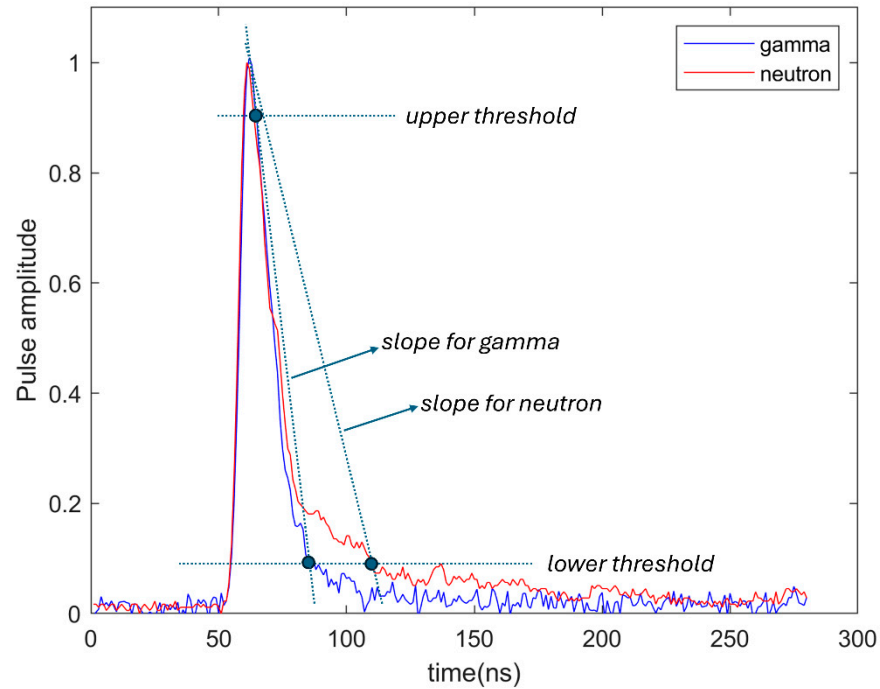


Figure 2. Scheme of the falling edge slope method: an upper threshold is selected, as well as a lower threshold for each pulse (as indicated on the picture). The slope is defined as the straight line between the two points. The steepest slope indicates a gamma-ray pulse.

A_{max} and its corresponding time t_0 are easy to determine by inspection of the pulse data. However, to obtain the unknowns τ and δA , there is a non-linear relationship, Equation (2). For all the data points in every pulse, it is possible to compose a system of equations of the form

$$Ax = k + r \tag{3}$$

where the A matrix (in bold, not to be confused with a particular amplitude A) and the independent term vector k have the forms

$$A = \begin{pmatrix} A_{max} \frac{\Delta t_1}{\tau_{approx}^2} e^{-\Delta t_1/\tau_{approx}} & \mathbf{1} \\ A_{max} \frac{\Delta t_2}{\tau_{approx}^2} e^{-\Delta t_2/\tau_{approx}} & \mathbf{1} \\ \dots & \dots \\ A_{max} \frac{\Delta t_n}{\tau_{approx}^2} e^{-\Delta t_n/\tau_{approx}} & \mathbf{1} \end{pmatrix} \tag{4}$$

$$k = \begin{pmatrix} A_1 - A_{max} e^{-\Delta t_1/\tau_{approx}} \\ A_2 - A_{max} e^{-\Delta t_2/\tau_{approx}} \\ \dots \\ A_n - A_{max} e^{-\Delta t_n/\tau_{approx}} \end{pmatrix} \tag{5}$$

for the unknown vector x

$$x = \begin{pmatrix} d\tau \\ \delta A \end{pmatrix} \tag{6}$$

and the vector of observation residuals r to be determined after the adjustment. Then the characteristic decay time and residual amplitude of the pulse will be

$$\tau = \tau_{approx} + d\tau \tag{7}$$

and δA , respectively.

In Equations (4) and (5), the amplitudes and times for data points $1, 2, \dots, n$ in a given pulse are used, that is, A_1, A_2, \dots, A_n , and $\Delta t_1, \Delta t_2, \dots, \Delta t_n$, respectively.

In this linearization, an approximate value τ_{approx} has been used. This approximate value can be set either by experience, or by inspection of the pulse shape in a first determination, which can also be subsequently improved by iteration: one simple strategy is to use a certain time Δt and the corresponding amplitude A (for example, one like the lower threshold in Figure 2) and then obtain τ from Equation (2) neglecting δA . Other values can be obtained by evaluating a few points just to obtain a suitable value to start the algorithm. Thus, for the current dataset, an approximate value of 12 ns is obtained. The selection of a poor approximate value will have an adverse effect on the results of the least squares adjustment but not so much on the results after robust estimation, due to its high insensitivity to systematic errors in the model.

The solution by *least squares* is simple and well-known:

$$x = (A^T A)^{-1} A^T k \tag{8}$$

$$r = Ax - k \tag{9}$$

$$C_x = \frac{r^T r}{n-2} (A^T A)^{-1} \tag{10}$$

where C_x is the covariance matrix of the unknowns, which has in the diagonal the squared values of the estimated standard errors of the unknowns, that is, σ_τ and $\sigma_{\delta A}$, respectively.

For solution by robust estimation, it is proposed to use the minimum L_1 -norm computed by a global optimization method: the simulated annealing method, which is based on the analogy with the self-construction process of crystalline networks. Instead of minimizing the sum of squared residuals, now, the objective is to find a solution that minimizes the L_1 -norm of residuals, that is, the function ρ defined as

$$\rho(r) = \sum_{i=1}^n |r_i| \tag{11}$$

To start the algorithm, an initial solution x_0 is selected (sensible choices are the approximate value for τ_{approx} mentioned before and zero for δA , or their corresponding values obtained after the least squares solution). Then a search domain centered on this initial solution is defined: a certain number of times, 3 or 5, the standard deviation of the least squares solution could be a possible choice to define the boundaries of the search domain. It has to be taken into account that a too large search domain will require a slower, more thorough, search, while an excessively small search domain might leave outside the global optimum that is sought for. An initial movement amplitude σ_0 (a vector with the standard deviation of the least squares solution for each unknown or similar values that could be used to explore all regions of the search domain in a few steps) is also set up. A final movement amplitude σ_{final} is also selected, with a size that can be considered negligible for the problem to solve ($\sigma_{final} = \sigma_0 / 100$ may be a reasonable choice). A cooling factor β with a value close to one (such as $\beta = 0.999$) has to be defined as well, taking into account that the closer to one the slower the optimization process (or, in the analogy, the cooling process of the solid hopefully becoming a crystalline network). Finally, a small probability

value p (such as $p = 0.01$) has to be selected to allow for the occasional selection of worse solutions (configurations of higher energy in the analogy).

With the initial solution x_0 , the residuals are computed by means of Equation (9) and the corresponding value for the objective function $\rho(r)$ is obtained by means of Equation (11). These values are stored as $x_{previous}$ and $\rho_{previous}$, respectively, to start the following iterative process. They are also stored as x_{best} and ρ_{best} . The initial movement amplitude is stored as $\sigma_{previous}$.

1. A new solution $x_{current}$ is obtained by taking the previous one as a base for a movement of amplitude $\sigma_{current}$, where

$$\sigma_{current} = \beta\sigma_{previous} \tag{12}$$

$$\Delta x \sim N(0, \sigma_{current}) \tag{13}$$

$$x_{current} = x_{previous} + \Delta x \tag{14}$$

and where the increment Δx has been taken from the multivariate normal distribution with zero mean and $\sigma_{current}$ standard deviation. It has to be checked that $x_{current}$ belongs to the search domain, otherwise a new solution in the search domain needs to be obtained again by Equations (13) and (14).

2. The residuals are computed by Equation (9) for the current solution and then, by Equation (11), the value for the objective function, $\rho_{current}$, is computed. If this value is smaller than the previous one $\rho_{previous}$, the current solution is selected as base solution for the next iteration (that is $x_{current}$ becomes $x_{previous}$ and $\rho_{current}$ becomes $\rho_{previous}$). Furthermore, if $\rho_{current}$ is smaller than ρ_{best} then $x_{current}$ is also stored as x_{best} and $\rho_{current}$ as ρ_{best} . Otherwise, if $\rho_{current}$ is not smaller than the previous one $\rho_{previous}$, then with the small probability p , the new solution is accepted as base solution or, otherwise, it is rejected so that the solution of the previous iteration is kept for the next iteration.

The process is stopped if the current movement amplitude $\sigma_{current}$ is smaller than the desired final movement amplitude σ_{final} . Otherwise, the algorithm turns back to step 1 above.

3. If the cooling process has been slow enough, at the end of the algorithm execution, the current solution must be coincident with the best solution (up to negligible differences of the order of σ_{final}). Furthermore, it is a necessary (though not sufficient) condition to attain the global minimum that repeated executions of the algorithm yield the same results (again, up to negligible differences of the order of σ_{final}).

More details on the application of the simulated annealing to the computation of this robust estimator can be found in [18]. Furthermore, the computer code given in the Supplementary Materials includes this algorithm.

2.3. Discrimination Performance Criteria

To evaluate the performance of neutron/gamma separation of the scintillator with the different methods, it is customary to use the figure of merit (FOM) value, which is given by

$$FOM = \frac{S}{FWHM_n + FWHM_\gamma} = \frac{|\mu_n - \mu_\gamma|}{2.35(\sigma_n + \sigma_\gamma)} \tag{15}$$

where S is the separation between neutron and gamma-ray maxima for the variable of the particular method (for example, the charge ratio in the case of the charge comparison method), and $FWHM_n$ and $FWHM_\gamma$ represent the full widths at half maximum of the neutron and gamma-ray contributions, respectively, Figure 3. Both components are assumed to be able to be adjusted by Gaussian functions, so that μ_n and μ_γ are the mean positions and σ_n and σ_γ are the standard deviations, respectively, of the neutron and the gamma ray contributions.

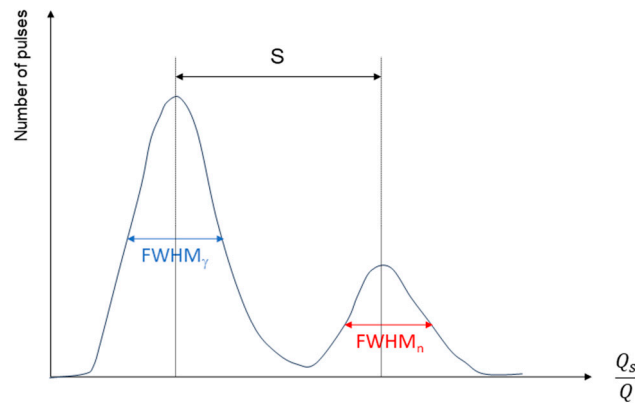


Figure 3. Scheme of FOM definition: the distance S between gamma and neutron contributions is evaluated, as the full widths at half maximum for each gamma and neutron lobes, respectively.

The crossing line (CL) to separate gamma-ray and neutron pulses can be set, following [11], as

$$CL = \frac{(\mu_\gamma + 3\sigma_\gamma) + (\mu_n - 3\sigma_n)}{2} \tag{16}$$

3. Results and Discussion

The determination of τ (characteristic decay time) and δA (residual amplitude) for each pulse, in accordance with Equation (2), will be used for discrimination between neutron and gamma pulses.

As a reference, the FOM value that is obtained with the charge comparison method for the same dataset (raw values) is taken. In [11], it is said that the FOM value for the application of the charge comparison method to this dataset is 1.3285, but a close inspection of the calculation of this value has revealed that a factor of $\ln(2)$ was missing in the denominator of their formula for FOM computation (QCSCM.m file); that is, 1.667 was used instead of 2.35 in Equation (15), so that the correct FOM value for the charge comparison method applied to this dataset is 0.9405.

First, the results obtained in each pulse for τ (in ns) and δA (unitless) in Equation (2) after their determination by standard least squares adjustments are presented. As can be seen in Figure 4, the values of τ alone obtained by least squares do not permit the separation of the neutron from gamma pulses: the corresponding FOM value is 0.4064.

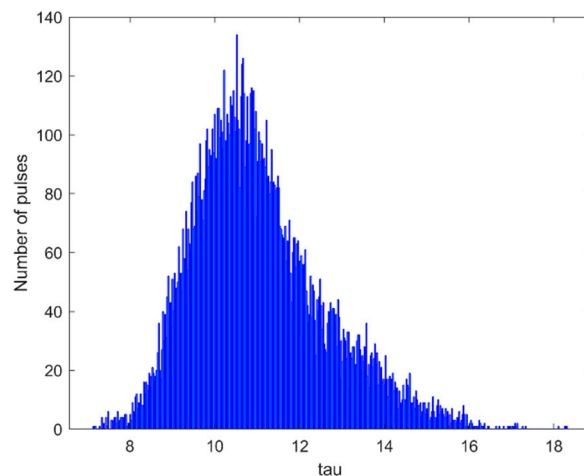


Figure 4. Discrimination by τ (τ) values obtained by least squares: the resulting FOM of 0.4064, associated by the visual fact that there is no clear distinction between gamma and neutron lobes, indicate a poor discrimination capability of the method. τ values in ns.

The τ values obtained by robust estimation allow for a better discrimination, Figure 5, but are still insufficient for a good separation; the FOM value is 0.6128.

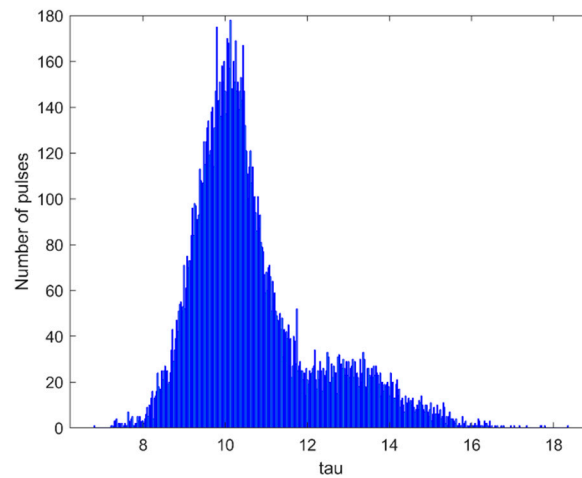


Figure 5. Discrimination by tau (τ) values obtained by robust estimation: a slightly better discrimination ability (FOM value 0.6128) than in the previous case is achieved. τ values in ns.

If the values of δA alone obtained by least squares and robust estimation are analyzed, Figures 6 and 7 are obtained, respectively, with corresponding FOM values of 0.9521 and 0.9525, which are very similar, and only slightly better than the value of 0.9405 obtained by the charge comparison method.

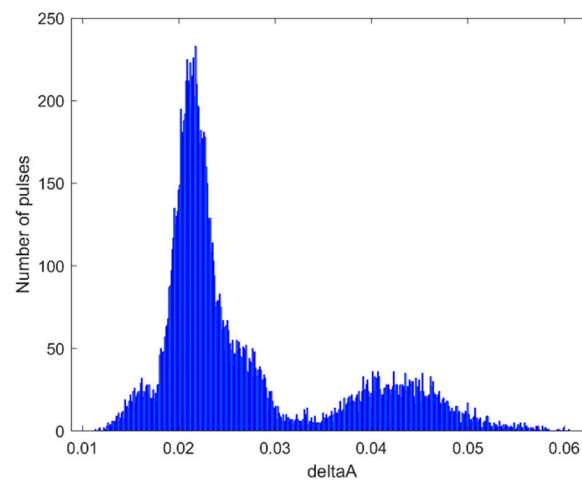


Figure 6. Discrimination by delta A (δA) values obtained by least squares. There is an evident separation between gamma and neutron contributions (the FOM value is 0.9521). δA values are unitless.

The fact that higher values for τ are obtained in the case of neutron pulses (values around 13 ns) than for gamma pulses (values around 11 ns) and, at the same time, higher values for δA are obtained in the case of neutron pulses (values around 0.044) than for gamma pulses (values around 0.024)—which can be explained by the above-mentioned contribution of the delayed emission—may suggest that the estimator obtained by multiplying the two, that is $\tau\delta A$, will provide a much better discrimination. In any case, having a look at the variances and covariances in the covariance matrix, it was observed that the correlation coefficient between τ and δA has an average (very stable) value of 0.4688. Thus, the variables are moderately correlated and it can be hoped that the discrimination can indeed be slightly enhanced by the combination of the two variables. The quantity $\tau\delta A$ obtained for each pulse after the estimation of τ and δA by least squares (Figure 8) and robust estimation (Figure 9) provides in effect, a much better discrimination between gamma

(lower values) and neutron (higher values) pulses. Their corresponding FOM values are 0.9265 and 1.0356, for the cases of least squares and robust estimation, respectively.

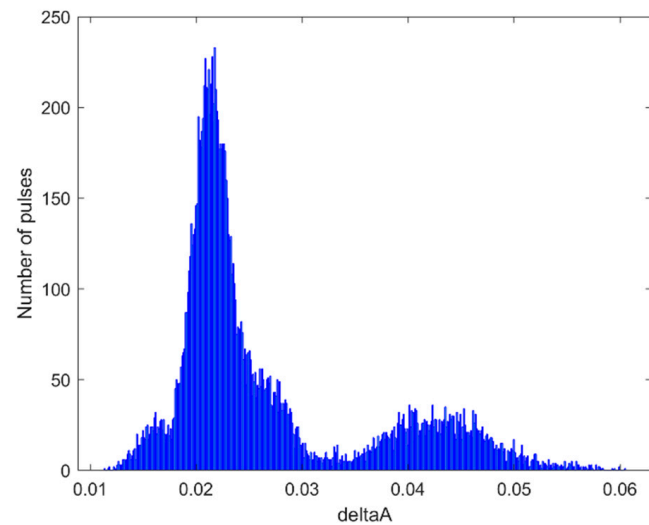


Figure 7. Discrimination by δA (δA) values obtained by robust estimation. The separation between gamma and neutron contributions is clearly observable (FOM value of 0.9525). δA values are unitless.

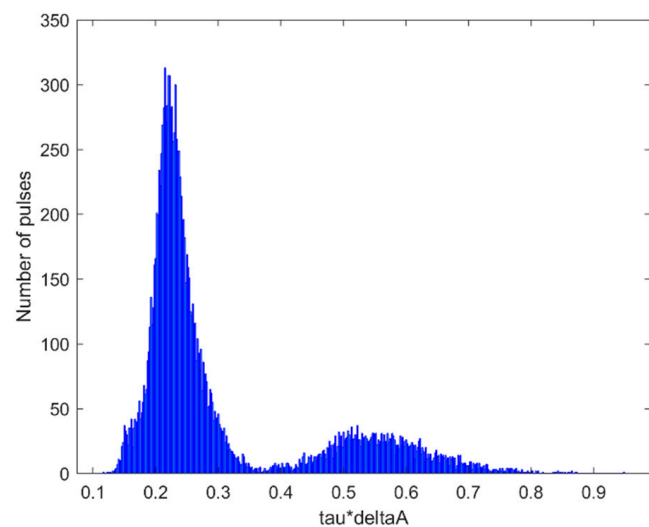


Figure 8. Discrimination by $\tau \delta A$ ($\tau \delta A$) values obtained by least squares. Gamma and neutron contributions are separated with a FOM value of 0.9265. $\tau \delta A$ values in ns.

Since the biggest difference between the results obtained by standard least squares and robust estimation occurs for the determination of the characteristic decay time (τ), one may suspect that this estimation is particularly difficult to obtain by least squares using a time window starting exactly at the peak, that is, using all the data points in the pulse with times equal or higher to the time where the maximum amplitude is found. If it is used for the determination of τ and δA , only a time window starting a few τ times after the peak, in a similar strategy to the time window for the computation of the Q_s value (Figure 1), the values estimated for the characteristic decay time (τ) by least squares improve indeed, with their results now being much similar than those obtained by robust estimation.

The values obtained for τ by least squares and robust estimation for a time window starting at $3\tau_{approx}$ (that is 36 ns) after each pulse peak are shown in Figures 10 and 11, respectively. They have FOM values of 0.6897 and 0.7614, respectively.

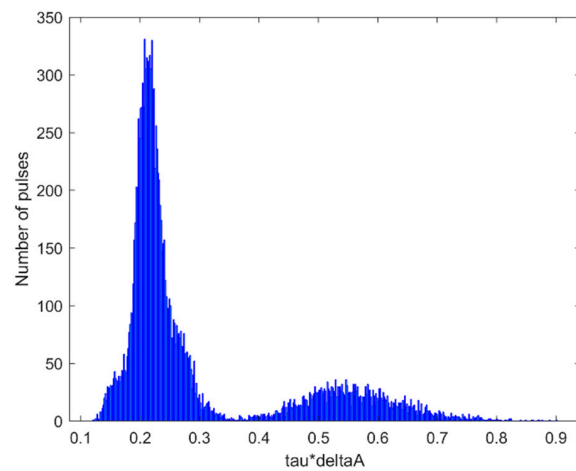


Figure 9. Discrimination by $\tau\delta A$ ($\tau\delta A$) values obtained by robust estimation. Gamma and neutron contributions are clearly separated with a FOM value of 1.0353. $\tau\delta A$ values in ns.

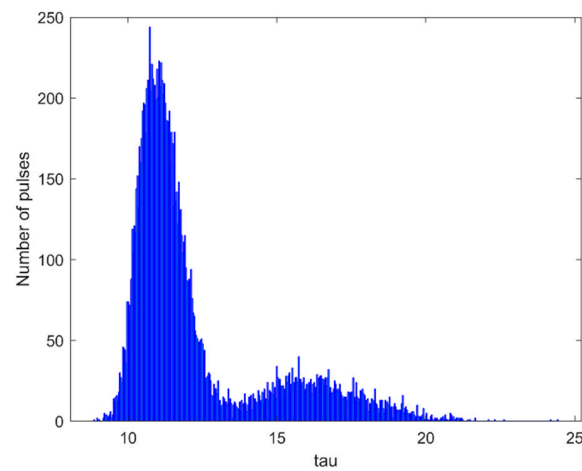


Figure 10. Discrimination by τ (τ) values obtained by least squares with a time window here chosen to be $3\tau_{approx}$, thus 36 ns. Evaluation of FOM gives 0.6897. As a reminder, the same method with no time window resulted in an FOM of 0.4064, with no clear separation between gamma-rays and neutrons (see Figure 4). τ values in ns.

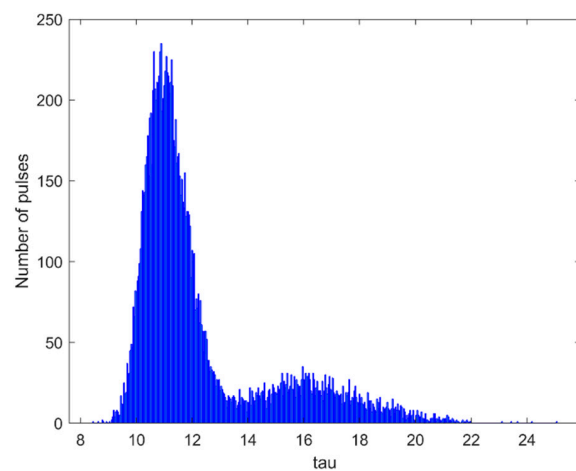


Figure 11. Discrimination by τ (τ) values obtained by robust estimation with a time window set at 36 ns ($3\tau_{approx}$), which gives an FOM value of 0.7614. The FOM previously evaluated with the same method but without a time window was 0.6128 (see Figure 5). τ values in ns.

The discrimination by the δA values obtained with the time window are shown in Figures 12 and 13, with the FOM values having worsened slightly for least squares (0.9089) and improved slightly for robust estimation (0.9973).

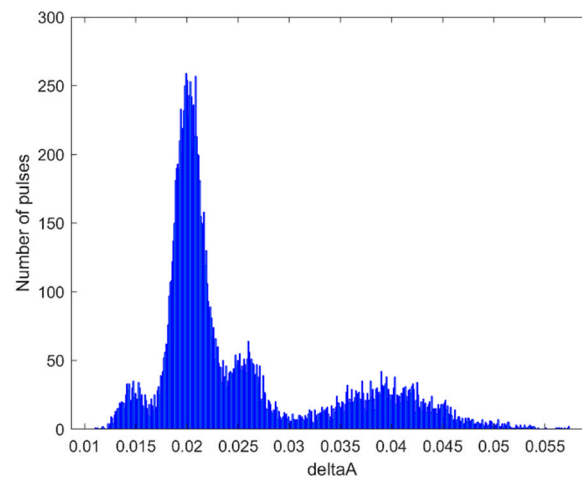


Figure 12. Discrimination by deltaA (δA) values obtained by least squares with a time window of 36 ns ($3\tau_{approx}$). The FOM value is 0.9089. The previous computation with no setup of a time window gave an FOM value of 0.9521 (see Figure 6). δA values are unitless.

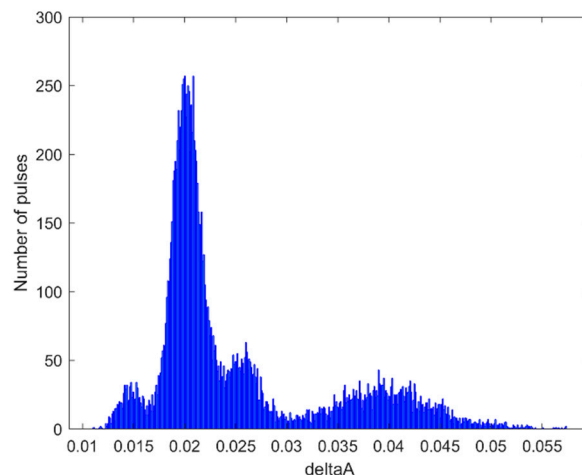


Figure 13. Discrimination by deltaA (δA) values obtained by robust estimation with a time window of 36 ns, which gives an FOM value of 0.9973. The same method without any use of a time window gave an FOM of 0.9525 (see Figure 7). δA values are unitless.

In these latter figures, Figures 12 and 13, the existence of other peaks apart from the main gamma peak (around 0.02) and the main neutron peak (around 0.04) became evident: those to the left and the right sides of the main gamma peak with respective peaks of around 0.015 and 0.025. These peaks were already present, though not so clearly visible in the previous Figures 6 and 7. The discussion of this phenomenon is deferred until the end of the section so as not to interfere with the current presentation of results since, as it will be shown, it is not caused by the method proposed.

Finally, the discrimination capabilities of $\tau\delta A$ after the estimation of τ and δA with the time window by least squares (Figure 14, FOM value of 0.9876) and robust estimation (Figure 15, FOM value of 0.9896) are similar; only slightly worse than the best results obtained without the time window, that is, those for $\tau\delta A$ by robust estimation.

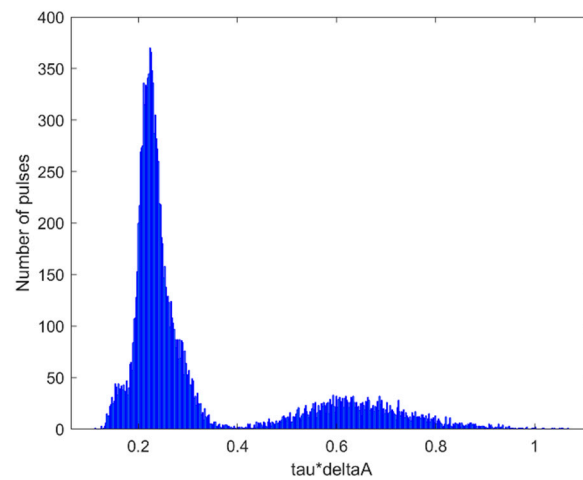


Figure 14. Discrimination by $\tau\delta A$ ($\tau\delta A$) values obtained by least squares with a time window of 36 ns, which gives an FOM value of 0.9876, instead of 0.9265 with no setup of time window (see Figure 8). $\tau\delta A$ values in ns.

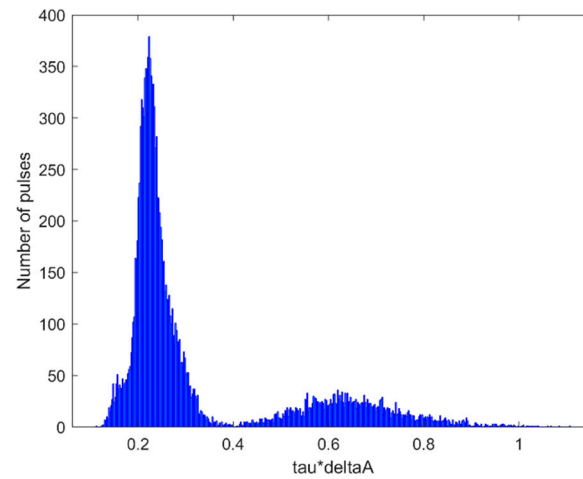


Figure 15. Discrimination by $\tau\delta A$ ($\tau\delta A$) values obtained by robust estimation with a time window of 36 ns. The FOM value is 0.9896, whereas it is 1.0356 with no time window (see Figure 9). $\tau\delta A$ values in ns.

The results obtained above are summarized in the following table of FOM values for the different approaches, Table 1. Those clearly improving the separation ability of the classical charge comparison method (FOM value 0.9405) come from $\tau\delta A$ computed by robust estimation (FOM value 1.0356), with moderate improvements over the charge comparison FOM for the $\tau\delta A$ obtained with the data window by least squares and robust estimation, and δA with the data window and robust estimation.

Table 1. FOM values for the different parameters computed, data windows and the two computation strategies: least squares (LS) and robust estimation (RE).

Parameters	Data Window	FOM Value after LS Computation	FOM Value after RE Computation
τ	All decaying parts	0.4064	0.6128
δA	All decaying parts	0.9521	0.9525
$\tau\delta A$	All decaying parts	0.9265	1.0356
τ	36 ns after the peak	0.6897	0.7614
δA	36 ns after the peak	0.9089	0.9973
$\tau\delta A$	36 ns after the peak	0.9876	0.9896

As a note of caution, it is highlighted the fact that the resulting uncertainties in τ and δA are around 0.01 and 0.05 times the respective values obtained in the adjustment, so, even if the FOM values above are given with four decimal places, differences of one percent or less in FOM values are not statistically significant.

The scatter plot for the best solution in terms of FOM value, that is, for the discrimination by $\tau\delta A$ with data from all the decaying parts by means of robust estimation, is given in Figure 16.

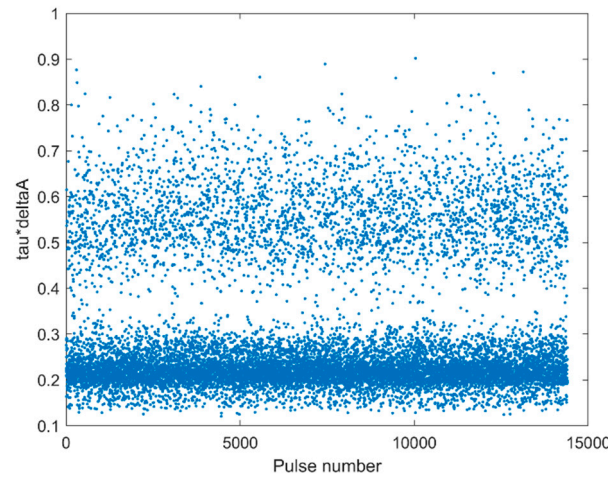


Figure 16. Scatter plot for $\tau\delta A$ by robust estimation and data from all the decaying parts. A clear separation between neutron and gamma-ray pulses can be seen.

The positive discrimination (PD) rates for gamma and neutron are also given for the different methods in Table 2. They account for the number of gamma (or neutron) pulses that were correctly classified according to the CL in Equation (16). As can be seen, the best approaches according to Table 1 are, in general, also delivering the best results in terms of PD rates. In particular, the best FOM resulted for $\tau\delta A$, determined by robust estimation from data for all decaying parts, which also gave the best PD rates: 0.9830 and 0.9968 for gamma and neutron, respectively.

Table 2. PD rates for gamma (γ) and neutron (n) for the different parameters computed, data windows and the two computation strategies: least squares (LS) and robust estimation (RE).

Parameters	Data Window	PD $_{\gamma}$ after LS Computation	PD $_n$ after LS Computation	PD $_{\gamma}$ after RE Computation	PD $_n$ after RE Computation
τ	All decaying parts	0.9123	0.6173	0.9174	0.9320
δA	All decaying parts	0.9517	0.9932	0.9268	0.9921
$\tau\delta A$	All decaying parts	0.9297	0.9926	0.9830	0.9968
τ	36 ns after the peak	0.8061	0.9762	0.9701	0.9864
δA	36 ns after the peak	0.8769	0.9926	0.9489	0.9077
$\tau\delta A$	36 ns after the peak	0.8946	0.9950	0.9479	0.9956

Now, it is time to discuss the origin of the two abnormal peaks in the δA plots, namely, those to the left and the right sides of the main gamma peak with respective peaks of around 0.015 and 0.025 (unitless), see Figures 12 and 13. It could be thought that they come from artifacts of the algorithm. However, a close inspection of the pulses whose δA values result around 0.015, say Area I, and those whose δA values result around 0.025, say Area II, reveals that the problem is coming from the dataset.

Figures 17 and 18 show two sample pulses having δA values around 0.015 (Area I, left of the main gamma peak), pulse numbers 98 and 348 in the dataset.

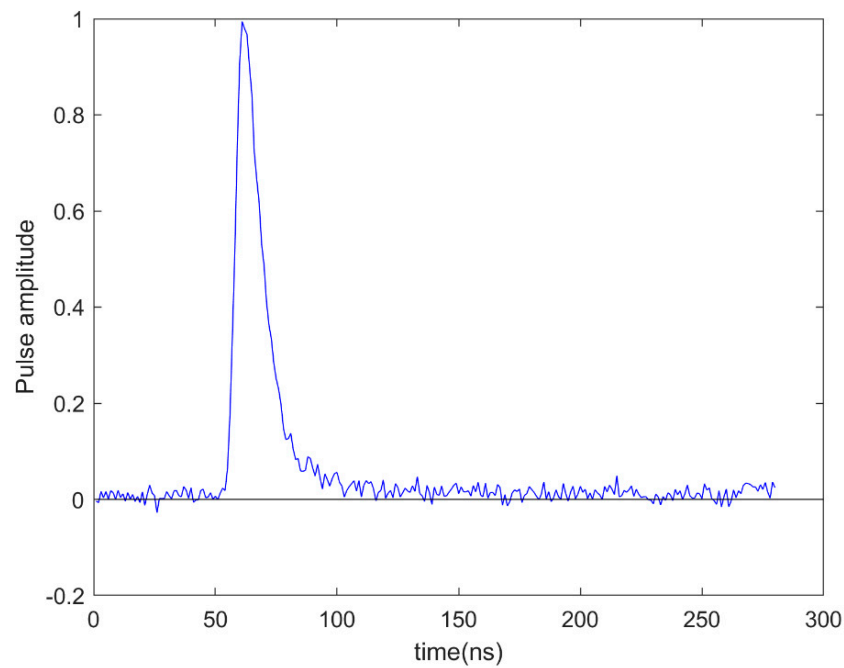


Figure 17. Amplitude of a first example pulse in Area I (peak to the left of the main gamma peak). Some amplitudes have negative values. Pulse amplitudes are unitless.

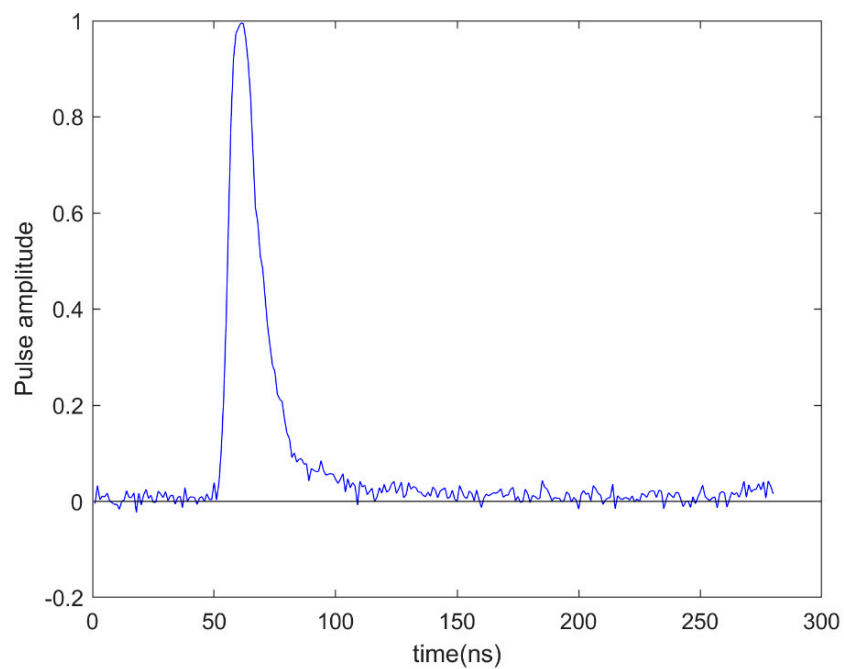


Figure 18. Amplitude of a second example pulse in Area I (peak to the left of the main gamma peak). Some amplitudes have negative values. Pulse amplitudes are unitless.

As said, the amplitudes in the dataset were said to be normalized between 0 and 1. However, this is clearly not the case of the pulses having δA values in Area I, since they have several values with negative amplitudes.

Similarly, two example pulses are shown in Figures 19 and 20 for δA values around 0.025 (Area II, right of the main gamma peak), pulse numbers 3371 and 5624 in the dataset.

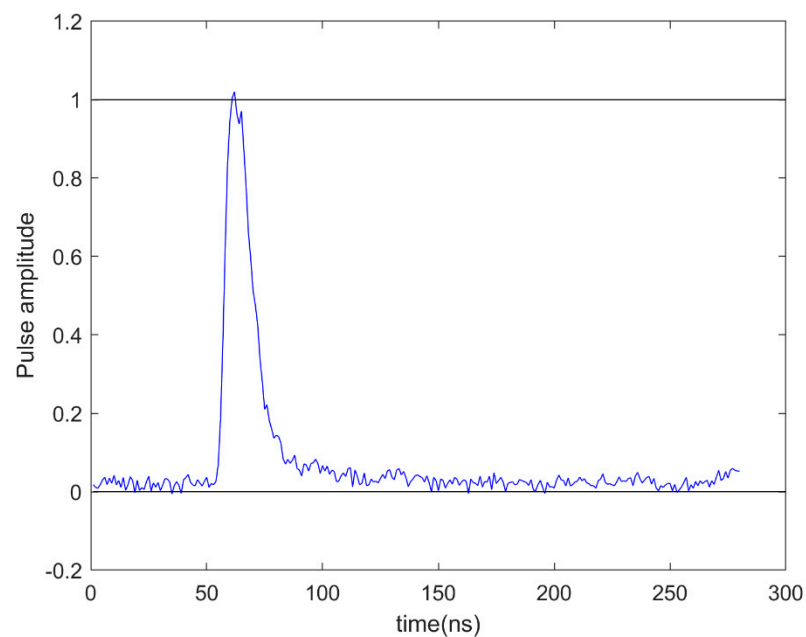


Figure 19. Amplitude of a first example pulse in Area II (peak to the right of the main gamma peak). The maximum amplitude exceeds 1. Pulse amplitudes are unitless.

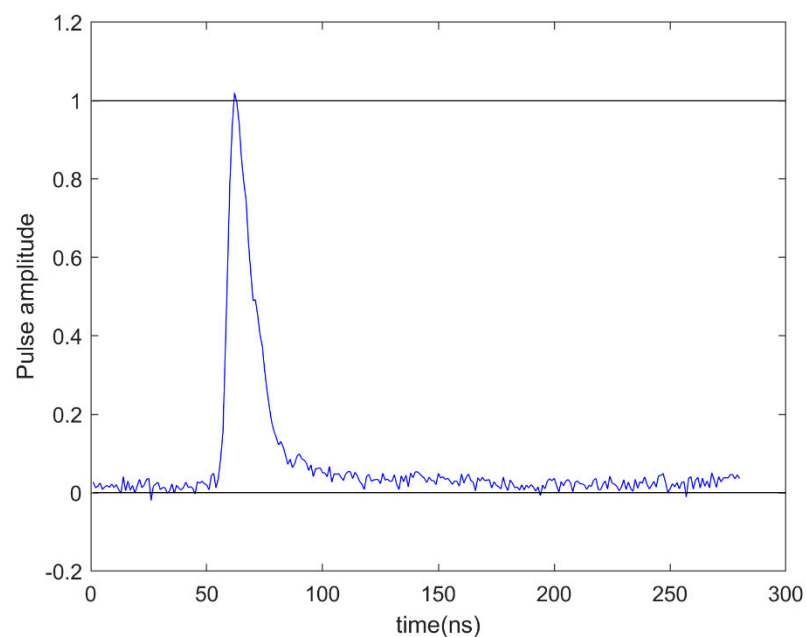


Figure 20. Amplitude of a second example pulse in Area II (peak to the right of the main gamma peak). The maximum amplitude exceeds 1. Pulse amplitudes are unitless.

Now, apart from a few values with negative amplitude, the most evident problem is that the supposedly normalized amplitudes surpass the value of 1. Also, in the very final part of the pulse, the amplitude seems to grow rather than decrease.

All these abnormalities could have been caused by undesired pulse reflections coming from cables and electronic components or by calibration issues. In any case, this cannot be known at this stage.

The Matlab computing codes, working along with the library and datasets given in [11], give the results for all decaying parts by least squares (S1) and robust estimation

(S2), and for the time window by least squares (S3) and robust estimation (S4) and are provided in the Supplementary Materials.

4. Conclusions

The robust determination of the decay shape as a new alternative for neutron/gamma discrimination has been proposed. It has been shown that the determination of the pulse shape in the decaying part by a robust estimation method can be used to successfully discriminate neutrons and gamma rays. For a given dataset, the corresponding FOM value improves on the FOM value of the standard charge comparison method by 10%. The determination of the pulse shape with a time window starting a little after the time of maximum amplitude can also provide satisfactory results, though of slightly lower quality, both by least squares and robust estimation. In terms of computing time, the robust estimation algorithm is around one order of magnitude slower than least squares, with computing times of tens of seconds instead of a couple of seconds for the dataset in use with a standard personal computer (Intel Core i5-12400 with 32 GB RAM). Additional research in order to test the proposed method (and the corresponding computing codes provided) in other datasets seems necessary to better assess its effectiveness.

Supplementary Materials: The following supporting information can be downloaded at: <https://www.mdpi.com/article/10.3390/app14135532/s1>, Computer code S1: Shape_discrimination_1.m, least squares results for all decaying part; Computer code S2: Shape_discrimination_2.m, robust estimation results for all decaying part; Computer code S3: Shape_discrimination_3.m, least squares results for the time window; Computer code S4: Shape_discrimination_4.m, robust estimation results for the time window.

Author Contributions: Conceptualization, E.M.; methodology, E.M. and S.B.; software, S.B.; validation, E.M. and S.B.; formal analysis, E.M. and S.B.; investigation, E.M. and S.B.; resources, S.B.; data curation, S.B. and E.M.; writing—original draft preparation, S.B. and E.M.; writing—review and editing, S.B. and E.M.; visualization, S.B.; supervision, E.M.; project administration, E.M. and S.B. All authors have read and agreed to the published version of the manuscript.

Funding: This research received no external funding.

Institutional Review Board Statement: Not applicable.

Informed Consent Statement: Not applicable.

Data Availability Statement: The data used for the study are openly available in Zenodo at <https://zenodo.org/records/7754573> (accessed on 20 June 2024).

Acknowledgments: The authors would like to express their gratitude for the preparation and release of the above-mentioned openly accessible dataset with more than 10,000 neutron gamma radiation pulse signals.

Conflicts of Interest: The authors declare no conflicts of interest.

References

1. Brooks, F.D.; Pringle, R.W.; Funt, B.L. Pulse Shape Discrimination in a Plastic Scintillator. *IRE Trans. Nucl. Sci.* **1960**, *7*, 35–38. [[CrossRef](#)]
2. Zaitseva, N.; Rupert, B.L.; Pawełczak, I.; Glenn, A.; Martinez, H.P.; Carman, L.; Faust, M.; Cherepy, N.; Payne, S. Plastic scintillators with efficient neutron/gamma pulse shape discrimination. *Nucl. Instrum. Methods Phys. Res. Sect. A Accel. Spectrom. Detect. Assoc. Equip.* **2012**, *668*, 88–93. [[CrossRef](#)]
3. Montbarbon, E.; Zhang, Z.; Grabowski, A.; Woo, R.; Tromson, D.; Dehé-Pittance, C.; Pansu, R.B.; Bertrand, G.H.V.; Hamel, M. The role of the secondary fluorophore in ternary plastic scintillators aiming at discriminating fast neutrons from gamma-rays. *J. Lumin.* **2019**, *213*, 67–74. [[CrossRef](#)]
4. Park, J.Y.; Mun, J.; Lee, J.H.; Yeon, Y.-H.; Chae, M.; Lee, M.; Lee, N.-H. Development of a Dual-Modality Gamma-ray/Fast Neutron Imaging System for Air Cargo Inspection. *Appl. Sci.* **2022**, *12*, 9775. [[CrossRef](#)]
5. Vasiljević, J.; Cederwall, B. Performance Evaluation of an Imaging Radiation Portal Monitor System. *Appl. Sci.* **2022**, *12*, 9001. [[CrossRef](#)]

6. Almisned, G.; Al-Abdullah, T.; Liadi, F.; Hawsawi, A. Improving a PGNAA Technique to Detect Heavy Metals in Solid Samples. *Appl. Sci.* **2022**, *12*, 3714. [[CrossRef](#)]
7. Almisned, G.; Tekin, H.O.; Zakaly, H.M.H.; Issa, S.A.M.; Kilic, G.; Saudi, H.A.; Algethami, M.; Ene, A. Fast Neutron and Gamma-Ray Attenuation Properties of Some HMO Tellurite-Tungstate-Antimonate Glasses: Impact of Sm³⁺ Ions. *Appl. Sci.* **2021**, *11*, 10168. [[CrossRef](#)]
8. Giuntini, L.; Castelli, L.; Massi, M.; Fedi, M.; Czelusniak, C.; Gelli, N.; Liccioli, L.; Giambi, F.; Ruberto, C.; Mazzinghi, A.; et al. Detectors and Cultural Heritage: The INFN-CHNet Experience. *Appl. Sci.* **2021**, *11*, 3462. [[CrossRef](#)]
9. Hawkes, N.P.; Gamage, K.A.A.; Taylor, G.C. Digital approaches to field neutron spectrometry. *Radiat. Meas.* **2010**, *45*, 1305–1308. [[CrossRef](#)]
10. Zaitseva, N.; Glenn, A.; Carman, L.; Hatarik, R.; Hamel, S.; Faust, M.; Schabes, B.; Cherepy, N.; Payne, S. Pulse Shape Discrimination in Impure and Mixed Single-Crystal Organic Scintillators. *IEEE Trans. Nucl. Sci.* **2011**, *58*, 3411–3420. [[CrossRef](#)]
11. Wang, K.; Liu, H.; Li, P.; Liu, M.; Zuo, Z. Dataset for neutron and gamma-ray pulse shape discrimination. *arXiv* **2024**, arXiv:2305.18242v3.
12. Lu, J.; Tuo, X.; Yang, H.; Luo, Y.; Liu, H.; Deng, C.; Wang, Q. Pulse-Shape Discrimination of SiPM Array-Coupled CLYC Detector Using Convolutional Neural Network. *Appl. Sci.* **2022**, *12*, 2400. [[CrossRef](#)]
13. Zuo, Z.; Xiao, Y.; Liu, Z.; Liu, B.; Yan, Y. Discrimination of neutrons and gamma-rays in plastic scintillator based on falling-edge percentage slope method. *Nucl. Instrum. Methods Phys. Res. Sect. A Accel. Spectrom. Detect. Assoc. Equip.* **2021**, *1010*, 165483. [[CrossRef](#)]
14. Maronna, R.A.; Martin, R.D.; Yohai, V.J. Robust Statistics: Theory and Methods. In *Wiley Series in Probability and Statistics*; John Wiley and Sons: Chichester, UK, 2006.
15. Yetkin, M.; Inal, C. L1 norm minimization in GPS networks. *Surv. Rev.* **2011**, *43*, 523–532. [[CrossRef](#)]
16. Baselga, S. Application of robust estimation methods to simple models of nucleon separation energies. *Mod. Phys. Lett. A* **2015**, *30*, 1550121. [[CrossRef](#)]
17. Suraci, S.S.; Oliveira, L.C.; Klein, I.; Goldschmidt, R.R. Optimal Minimum L1-Norm Criteria for Outlier Identification in GNSS and Leveling Networks. *J. Surv. Eng.* **2023**, *149*, 04023016. [[CrossRef](#)]
18. Baselga, S. Global Optimization Solution of Robust Estimation. *J. Surv. Eng.* **2007**, *133*, 123–128. [[CrossRef](#)]
19. Batilović, M.; Đurović, R.; Sušić, Z.; Kanović, Ž.; Cekić, Z. Robust Estimation of Deformation from Observation Differences Using Some Evolutionary Optimisation Algorithms. *Sensors* **2022**, *22*, 159. [[CrossRef](#)] [[PubMed](#)]

Disclaimer/Publisher's Note: The statements, opinions and data contained in all publications are solely those of the individual author(s) and contributor(s) and not of MDPI and/or the editor(s). MDPI and/or the editor(s) disclaim responsibility for any injury to people or property resulting from any ideas, methods, instructions or products referred to in the content.